CrossMark
click for updates

View Article Online
View Journal

Metallomics

Accepted Manuscript

This article can be cited before page numbers have been issued, to do this please use: M. Cini, H. Williams, M. W. Fay, M. Searle, S. Woodward and T. D. Bradshaw, *Metallomics*, 2016, DOI: 10.1039/C5MT00297D.

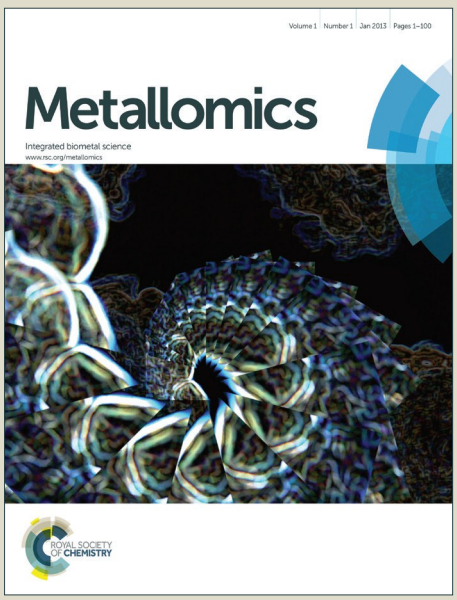

This is an *Accepted Manuscript*, which has been through the Royal Society of Chemistry peer review process and has been accepted for publication.

Accepted Manuscripts are published online shortly after acceptance, before technical editing, formatting and proof reading. Using this free service, authors can make their results available to the community, in citable form, before we publish the edited article. We will replace this *Accepted Manuscript* with the edited and formatted *Advance Article* as soon as it is available.

You can find more information about *Accepted Manuscripts* in the Information for Authors.

Please note that technical editing may introduce minor changes to the text and/or graphics, which may alter content. The journal's standard Terms & Conditions and the Ethical guidelines still apply. In no event shall the Royal Society of Chemistry be held responsible for any errors or omissions in this *Accepted Manuscript* or any consequences arising from the use of any information it contains.

ROYAL SOCIETY OF CHEMISTRY

www.rsc.org/metallomics

View Article Online
DOI: 10.1039/C5MT00297D

Enantiopure titanocene complexes - direct evidence for paraptosis in cancer cells

Melchior Cini,[a,b,c,d] Huw Williams,[a,d] Mike W. Fay,[c] Mark S. Searle,[a,d] Simon Woodward,[a,] and Tracey D. Bradshaw,[b,d].

[a] School of Chemistry, University of Nottingham, University Park, Nottingham NG7 2RD, United Kingdom.

[b] School of Pharmacy, Centre for Biomolecular Sciences, University of Nottingham, University Park, Nottingham NG7 2RD, United Kingdom.

[c] Nottingham Nanotechnology and Nanoscience Centre, University of Nottingham, University Park, Nottingham NG7 2RD, United Kingdom.

[d] Centre for Biomolecular Sciences, University of Nottingham, University Park, Nottingham, NG7 2RD, United Kingdom.

To whom correspondence may be addressed. Email: simon.woodward@nottingham.ac.uk; tracey.bradshaw@nottingham.ac.uk; melchior.cini@nottingham.ac.uk

Published on 18 January 2016. Downloaded by University of Nottingham on 18/01/2016 16:44:32.

Abstract

Tolerated by normal tissues, anti-cancer therapies based on titanium compounds are limited by low efficacy/selectivity and lack of understanding of their mode(s) of action. *In vitro* antitumour activity and mode of cell death incurred by enantiopure $TiCl_2\{\eta\text{-}C_5H_4CHEt(2\text{-}MeOPh)\}_2$ (abbreviated $Cp^R{}_2TiCl_2$) has been investigated. The *in vitro* anti-tumour activity of $Cp^R{}_2TiCl_2$ is selective for cancer cells; in clonogenic assays, (*S*,*S*)-$Cp^R{}_2TiCl_2$ was twice as effective at inhibiting colony formation than other stereoisomers after 24 h exposure. HPLC, MS and NMR techniques determined hydrolysis of $Cp^R{}_2TiCl_2$; data strongly correlate with soluble $[Cp^R{}_2Ti(OH)(OH_2)]^+$ being the biological trigger. Treatment of cells with $Cp^R{}_2TiCl_2$ provoked extensive cytoplasmic vacuolization, endoplasmic reticulum (ER) swelling and activation of MAPKinase signal transduction, consistent with ligand-induced paraptosis, type III cell death, which is morphologically distinct from, and independent of apoptosis. Indeed, distinct from cisplatin, $Cp^R{}_2TiCl_2$ failed to perturb cell cycle dynamics, induce γH2AX foci or evoke apoptosis in MDA-MB-468 and HCT-116 cells.

Titanocenes | chiral cyclopentadienyls | paraptosis | cancer | MDA-MB-468

Introduction

Pioneering work more than 30 years ago revealed the antiproliferative properties of titanocene dichloride (Cp_2TiCl_2; **1**) and analogous titanocene complexes[1] in tumour models *in vitro* and *in vivo*. Cp = η-C_5H_5 is a cyclopentadienyl ligand; Cp_2TiCl_2 was the first non-platinum coordination complex and the first metallocene to be investigated as an anticancer drug. It underwent phase 1 clinic trials in adults with advanced solid tumors in 1993[2,3,4]. Although Cp_2TiCl_2 was tolerated, dose-limiting adverse reactions, attributed to

Metallomics Accepted Manuscript

View Article Online
DOI: 10.1039/C5MT00297D

nephrotoxicity, hypoglycemia and nausea were encountered; however, the absence of myelosuppression, a common chemotherapeutic dose-limiting toxicity was intriguing, enhancing the medical applicability of this agent. Low antitumour efficacy in Phase 2 studies discouraged further development of this agent[5, 6].

Interest in titanocenes has been renewed with synthesis and evaluation of novel analogues exemplified by [{η-$C_5H_4(CH_2C_6H_4OCH_3)$}$_2TiCl_2$] (titanocene Y, **3**) which demonstrated anticancer efficacy in human xenograft studies[7]. Substituted *chiral* titanocenes (e.g. **4**) are thought to offer even greater efficacy but are seldom used due to inherent formation of mixures of stereoisomeric titanium complexes which complicates their study (Figure 1).

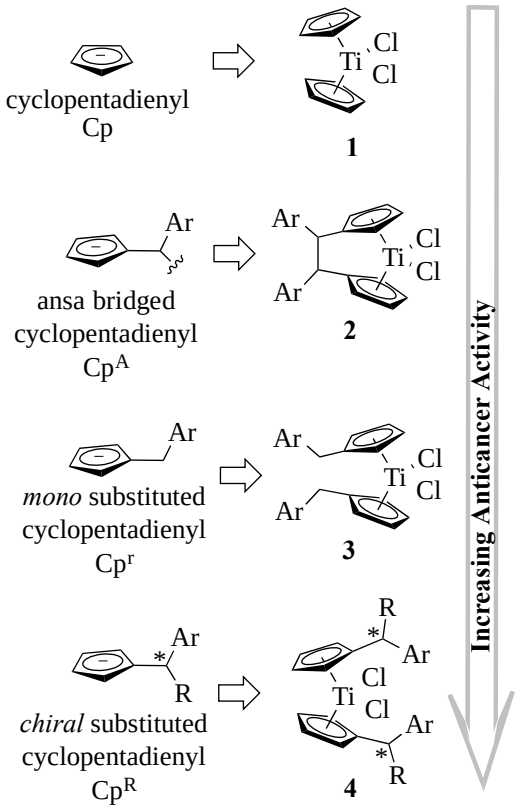

Figure 1. Cyclopentadienyls and titanocenes discussed in this paper. For titanoncene Y: Ar = 4-$MeOC_6H_4$. For our own chiral titanocene **4**: Ar = 2-$MeOC_6H_4$; R = Et; the chiral centres of **4** are show by '*'.

The anticancer mechanisms of titanocene dichloride complexes are not fully understood. It has been conjectured that activity is attributable to the compounds` interactions with the protein transferrin[8-11]. It has also been suggested that DNA may be the target for titanocene-based agents as titanium-DNA adducts were detected in A2780 cells treated with titanocene dichloride[12]. However, experiments have indicated alternative mechanisms of action and cell death following detection of ligand-bound Ti(IV) complexes to other proteins (e.g. albumin) or proteolytic enzymes[13, 14]. Recently described has been the potent and selective anticancer activity of organometallic-titanocene compounds, but lack of interaction between compounds and plasmid DNA implicated alternative biomolecular targets; accordingly, AKT and MAP kinase family protein kinase activity was inhibited[15].

Published on 13 January 2016. Downloaded by University of Nottingham on 18/01/2016 16:44:32.

Metallomics Accepted Manuscript

View Article Online
DOI: 10.1039/C5MT00297D

Hydrolytic instability in titanocenes, a consequence of initial loss of chloride, and potentially cyclopentadienyl-Ti cleavage, can provide a cocktail of species which is further complicated in chiral substrates. Multiple stereoisomers result unless single enantiomers of the chiral cyclopentadienyl ligands are used. Disentangling the relative biological activities of such mixtures is not normally possible. Recently, the enantio-enriched cyclopentadienyl fragment $C_5H_4CHEt(2\text{-}MeOPh)$ (abbreviated Cp^R) needed for the synthesis of enantiopure (*S,S*)-**4** was attained by unprecedented copper-catalyzed asymmetric $ZnEt_2$ addition to the exo-alkene of pentafulvene[16]. Such catalytic stereoselective addition of organometallics to pentafulvenes was previously unknown, preventing ready access to the desired biological probes.

Herein we describe *in vitro* biological and biophysical studies of separated (*R,R*)- and (*S,S*)-**4** enantiomers (Figure 1); determining whether cyclopentadienyl hydrolysis, and hence Ti^{4+} formation, is a prerequisite for biological activity; a question of contemporary interest[17].

Results and Discussion

Biology

MTT assays were used to determine growth inhibitory properties of (*S,S)*- and (*R,R)*-**4** enantiomers. Preliminary data revealed statistical ($P<0.05$) differential growth inhibitory activity following 24 h exposure of cancer cells to the enantiopure agents (*S,S*) *vs*. (*R,R*)-**4**[16]. However, after 72 h treatment, negligible selectivity between the stereoisomers of **4** was observed (Table 1). Intriguingly following 72 h treatment, all isomers of **4** demonstrated significant selectivity (between 2- and 5-fold; $P<0.05$) for cancer cell lines screened (e.g. $GI_{50}<6$ μM; MDA-MB-468) over non-transformed MRC5 fibroblasts ($GI_{50}>25$ μM). Such behavior raises questions concerning the aqueous speciation of **4** as a function of time (see biophysics later). The behavior of **4** is in contrast to cisplatin which showed no selectivity towards cancer cells (equipotency against Mia PaCa-2, HCT-116 carcinoma cells and MRC-5 fibroblasts; with GI_{50} 6-8 μM; Figure S1, 72 h).

	GI_{50} value (μM) mean ± SD			
Cell line	(*R,R*)-**4**	(*S,S*)-**4**	(*rac/meso*)-**4**	Cisplatin
MiaPaCa-2	7.3 ± 0.5	5.7 ± 1.3	7.5 ± 0.4	5.8 ± 0.7
MDA-MB-468	5.6 ± 1.8	5.4 ± 1.3	5.3 ± 1.7	2.1 ± 0.6
HCT 116	14.0 ± 2.1	9.4 ± 1.2	12.2 ± 3.9	7.9 ± 0.5
MRC5	25.1 ± 3.5	28.3 ± 5.0	28.6 ± 3.7	8.3 ± 3.1

Table 1. Effect of Titanocene analogues and cisplatin in growth of carcinoma cells and fibroblasts in culture. Cells were exposed to test agent for 72 h before cell growth was determined by MTT assay. Mean GI_{50} values (μM) were calculated from ≥3 independent trials (n = 8 per trial).

Published on 18 January 2016. Downloaded by University of Nottingham on 18/01/2016 16:44:32.

Metallomics Accepted Manuscript

View Article Online
DOI: 10.1039/C5MT00297D

Assays testing subsequent colony growth following 24 h exposure of single HCT 116 or Mia PaCa-2 cells to (*S*,*S*) or (*R*,*R*)-**4** (20-50 μM) support ~2× differential enantiomer activity. For example, compared to control, 22% vs 46% HCT 116 survival and subsequent colony formation was determined in cells exposed to (*S*,*S*)-**4** and (*R*,*R*)-**4** (24 h) respectively (Figure 2).

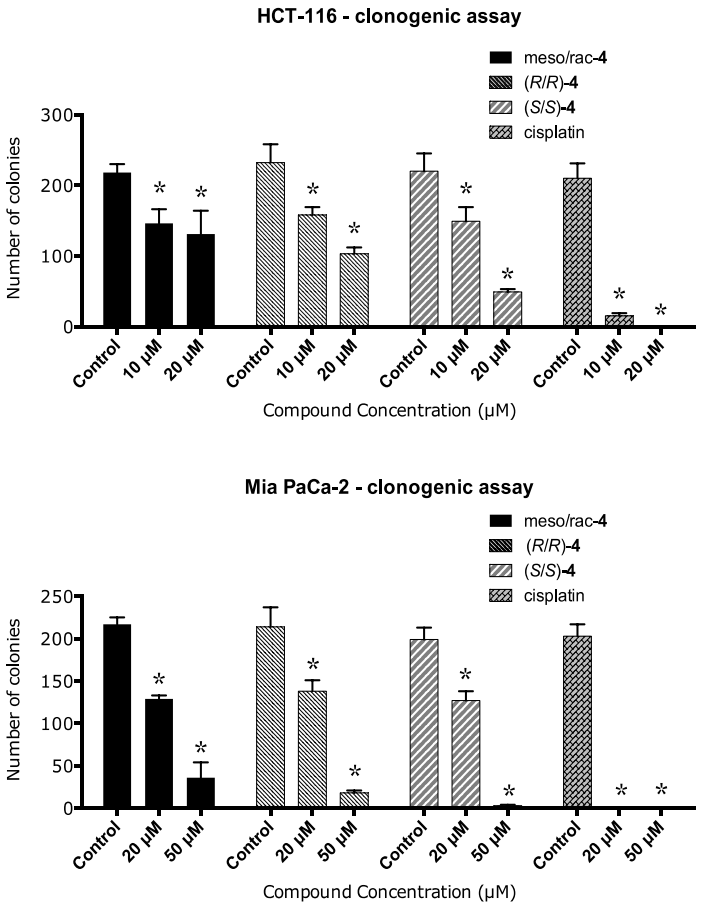

Figure 2. Effects of cisplatin and titanocene derivatives on HCT 116 and Mia PaCa-2 cell survival and colony formation following 72 h exposure to test agent. Colonies were fixed, stained and counted (n=6); 2 independent trials. *p<0.05 significant difference from control; 2 way ANOVA, multiple comparisons.

Cell cycle analyses, γH2AX foci and apoptosis

Examination of cell cycle distribution revealed that in stark contrast to cisplatin, titanium based (*S*,*S*)-**4** negligibly perturbed MDA-MB-468 or HCT 116 cell cycle (±5% of control values; Figure 3).

After 24 h treatment (MDA-MB-468; (*S*,*S*)-**4**), gap 2 and mitotic (G2/M) events were marginally elevated, but at 72 h exposure, negligible increases in pre-gap 1 (G1) and G1 populations were encountered at the expense of G2/M events. Only after 72 h exposure of MDA-MB-468 cells to 20 μM (*S*,*S*)-**4** was a minor increase (≤5%) in sub-G1 events detected. Cisplatin however (10 μM; 24 h and 72 h) caused significant accumulation of pre-G1 phase events (e.g. 28% and 60% total MDA-MB-468 population respectively). In HCT 116 cells, (*S*,*S*)-**4** (20 μM; 72 h) did not increase the sub-G1 population, the only notable change was a slight decrease in S phase events – the period during which DNA is copies (DNA synthesis).

Published on 18 January 2016. Downloaded by University of Nottingham on 18/01/2016 16:44:32.

Metallomics Accepted Manuscript

View Article Online
DOI: 10.1039/C5MT00297D

Cisplatin, in contrast, evoked significant and marked rises in G2/M phase events in HCT 116 cells (24 h and 72 h; 15 μM and 25 μM); at 72 h, substantially significant subG1 events were detected (indicative of apoptosis; Figures 3 and 4Ciii).

G2/M arrest would be expected of a DNA-damaging agent and cisplatin is known to form DNA intra-strand cross links, mono-adducts, inter-strand crosslinks, and DNA-protein crosslinks. Mostly it acts on adjacent N-7 guanine forming 1, 2 intra-strand crosslinks[18,19]. HCT 116 cells possess wild type P53, a tumour suppressor gene whose protein product has key roles in DNA damage detection, cell cycle arrest and DNA repair, or apoptosis initiation in the face of irreparable DNA damage[20]. MDA 468 cells harbour mutant P53; in these cells, we fail to detect G2/M cell cycle arrest, however, hugely significant preG1 populations emerge. It may be surmised that in the absence of functional P53 and G2/M arrest, DNA repair mechanisms are not initiated and the preG1 populations observed following treatment of cells are indicative of apoptosis. Following treatment of cells with titanocene (*S*,*S*)-**4** , significant cell cycle perturbation was clearly absent (Figure 4Cv), therefore there is no evidence to suggest titanocene **4** causes DNA damage resulting in apoptosis induction.

Titanocene Y (**3**) has been reported to reduce clonogenic survival, cause DNA damage and dose-dependent apoptosis in prostate cancer cells, but did not affect the cell cycle[21]. O`Connor *et al*. report that **3** caused significant prostate cell cycle effects and apoptosis[22]. However, these authors concluded a caspase-independent mode of cell death when the pan caspase inhibitor ZVAD-FMK failed to inhibit apoptosis. Titanocene dichloride **1** triggered A2780 ovarian carcinoma cell cycle arrest in late S, early G_2 cell cycle phase, formation of Ti-DNA adducts and apoptosis[12]. To determine whether (*S*,*S*)-**4** caused DNA damage leading to double strand breaks (DSBs), we investigated generation of γH2AX. Histone H2AX is phosphorylated by kinases (such as ATM and ATR) at sites of DNA DSBs 1:1[23].

Dual γH2AX / cell cycle analyses further corroborated the thesis that titanocene analogue **4** failed to evoke DNA damage resulting in double strand breaks. In neither MDA-MB-468 nor HCT 116 cells exposed for 72 h to 10 μM or 20 μM (MDA-MB-468) 20 μM or 30 μM (HCT 116) (*R*,*R*)-**4** or (*S*,*S*)-**4** were significant γH2AX foci generated (Figure 4A and B). In contrast, significant DNA damage was detected in cells (MDA-MB-468 or HCT 116) exposed to cisplatin (5 μM; 10 μM or 15 μM; 25 μM respectively; $P<0.05$)). Particularly striking were the numbers of γH2AX positive events within the G2/M cell cycle phase of cisplatin treated HCT 116 populations (exemplified in Figure 4Ciii and iv; 15 μM; 72 h). Contrast this with the γH2AX (and cell cycle) profile of HCT 116 cells exposed to 30 μM (*S*,*S*)-**4**; 72 h, which is indistinct from control (Figure 4Cv and vi).

Published on 18 January 2016. Downloaded by University of Nottingham on 18/01/2016 16:44:32.

Metallomics Accepted Manuscript

View Article Online
DOI: 10.1039/C5MT00297D

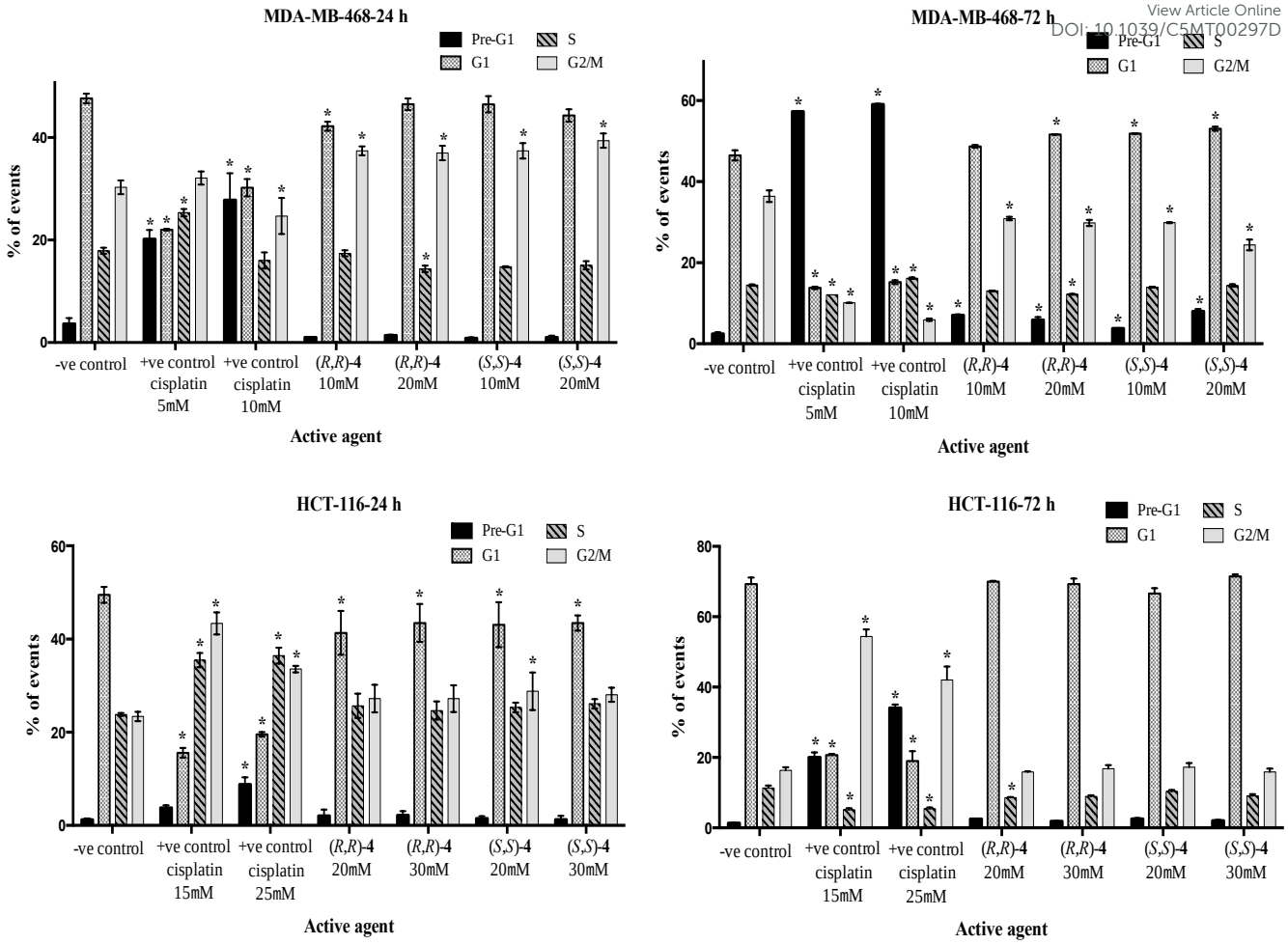

Figure 3. Effects of cisplatin, (*R,R*)-**4** and (*S,S*)-**4** on MDA-MB-468 and HCT 116 cell cycle distribution. Data represent ≥3 independent trials (n=2 per trial; 20,000 events analyzed per sample). *p<0.05 significant difference from control; 2 way ANOVA, multiple comparisons. In contrast to cisplatin which significantly increases preG1 cell cycle events, titanocenes (*R,R*)-**4** and (*S,S*)-**4** fail to dramatically perturb cell cycle distribution.

DNA detected in the subG1 cell cycle phase is indicative of caspase-mediated apoptosis. SubG1 MDA-MB-468 and HCT 116 events were evident following exposure of cells to cisplatin; small but significant subG1 populations were observed in MDA-MB-468 cells exposed to 10 μM (*S,S*)-**4**; 72 h. To determine whether apoptosis had been induced, cells were subject to dual PI/annexin V staining before analyses by flow cytometry. An early event during apoptosis is loss of membrane asymmetry. Phosphatidylserine (resident on the inner cell membrane leaflet) becomes exposed and binds annexin V. As apoptosis progresses to late phase, membrane integrity is lost allowing cell membrane penetration of PI.

Bannon *et al*. demonstrated cell cycle perturbation and late apoptotic A431 epidermoid carcinoma cell populations following exposure to cisplatin or titanocene Y (**3**; 50 μM; 48 h)[24], indicative of caspase-induced apototosis. Similarly, gene expression analysis in small cell lung cancer cells treated with related species was in accord with DNA damage being the apoptosis trigger[25].

Published on 18 January 2016. Downloaded by University of Nottingham on 18/01/2016 16:44:32.

Metallomics Accepted Manuscript

View Article Online
DOI: 10.1039/C5MT00297D

Published on 18 January 2016. Downloaded by University of Nottingham on 18/01/2016 16:44:32.

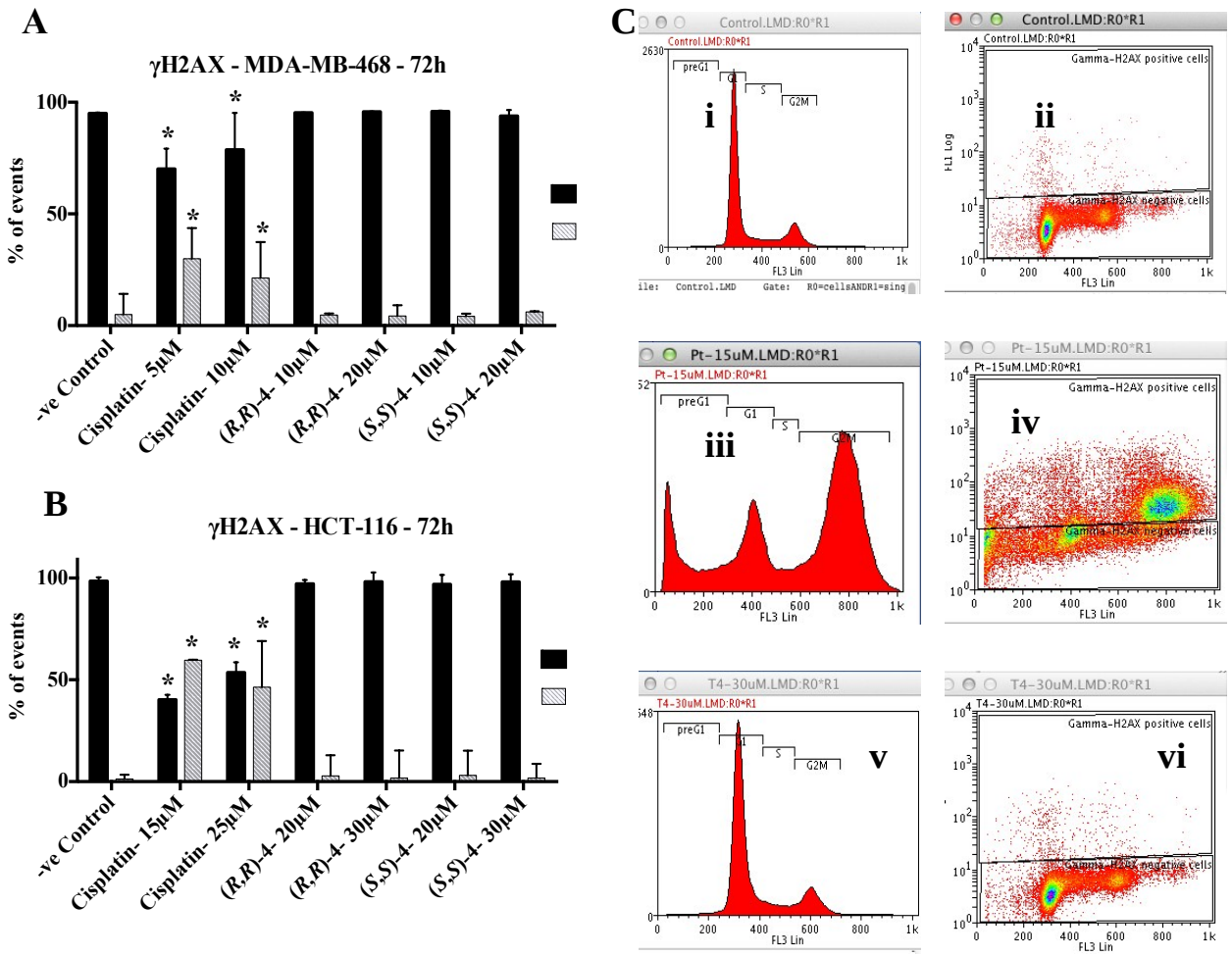

Figure 4. Determination of DNA double strand breaks by flow cytometric analyses of γH2AX cells following 72 h treatment of A) MDA-MB-468 or B,C) HCT 116 cells with cisplatin, (*R*,*R*)-**4** and (*S*,*S*)-**4** enantiomers. Data represent ≥3 independent trials (n=2 per trial; 20,000 events analyzed per sample). *p<0.05 significant difference from control; 2 way ANOVA, multiple comparisons. C) Representative analyses of HCT 116 cells demonstrating concurrent cell cycle distribution (i, iii, v) and γH2AX positive events (ii, iv, vi) following exposure of cells to vehicle (i, ii), 15 μM cisplatin (iii, iv) or 30 μM (*S*,*S*)-**4** (v. vi).

As is shown in Figure 5, cisplatin (5 μM and 15 μM) triggered significant MDA-MB-468 and HCT 116 cellular apoptosis (~60% and ~30% respectively; P<0.05), consistent with cell cycle predictions. In contrast, following 72 h exposure of cells to (*R*,*R*)-**4** and (*S*,*S*)-**4** titanocene enantiomers, significant annexin V+ (apoptotic) populations were detected only in MDA 468 cells treated with 20 μM (*S*,*S*)-**4** and (*R*,*R*)-**4**. Again, corroborating cell cycle analyses, cells undergoing titanocene-induced apoptosis represented a minority population (<10%).

Metallomics Accepted Manuscript

View Article Online
DOI: 10.1039/C5MT00297D

Based on our evidence, the hypothesis that (*R*,*R*)-**4** and (*S*,*S*)-**4** evoke anticancer activity, DNA damage and cell death through apoptosis was rejected. Indeed, features characteristic of apoptosis – chromatin condensation, nuclear fragmentation, cytoplasmic shrinkage, apoptotic membrane blebbing, formation of apoptotic bodies – were absent (TEM, confocal microscopy). However, other dramatic cellular morphological modifications were induced by **4** (the timing of which was concurrent with maximized concentrations of intermediate $[Cp^{R}_{2}Ti(OH)(OH_2)]^{+}$; <6 h; as explained later).

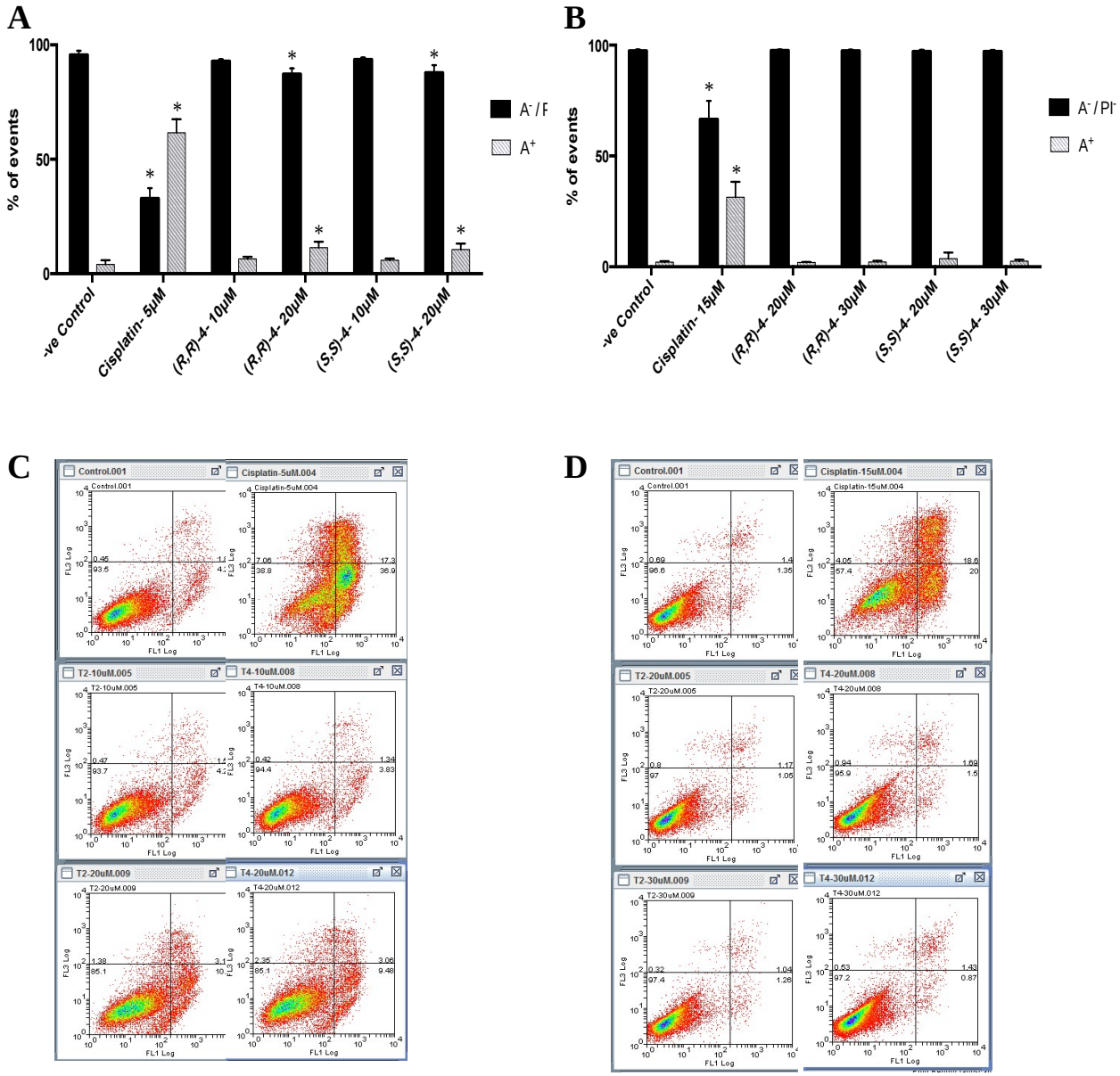

Figure 5. Effects of cisplatin and titanocene derivatives on MDA-MB-468 (A, C) and HCT 116 (B, D) apoptosis. Cells were exposed to test agent for 72 h and prepared for flow cytometric analyses following dual annexin V, PI staining. A, B) Cells undergoing apoptosis were defined as the sum of early apoptotic (annexin V +ve) and late apoptotic (annexin V +ve, PI +ve) populations. Data represent ≥3 independent trials (n=2 per trial; 20,000 events analyzed per sample). *p<0.05 significant difference from control; 2 way ANOVA, multiple comparisons. Representative analyses of MDA-MB-468 (C) and HCT 116 (D) apoptotic

Published on 18 January 2016. Downloaded by University of Nottingham on 18/01/2016 16:44:32.

Metallomics Accepted Manuscript

View Article Online
DOI: 10.1039/C5MT00297D

populations following 72 h exposure of cells to: i) vehicle; ii) 15 μM cisplatin; iii) 20 μM (*R,R*)-**4**; iv) 30 μM (*R,R*)-**3**; v) 20 μM (*S,S*)-**4**; vi) 30 μM (*S,S*)-**4**.

Induction of Paraptosis

Titanocene **4** induced rapid (<6 h), distinctive changes in cellular morphology; extensive cytoplasmic vacuolization became evident in cells exposed to (*S,S*)-**4** (20 μM - 0-13 h. Confocal microscopy time-image studies of live MDA-MB-468 cells reveal ER swelling (0.33-66 h, Figure S4A) and crater-like cups on the cell surface (Supplementary Information movie; Figure 6A). This is followed by vacuole membrane rupture (osmotic lysis) and cell death. After the highest practical exposure of MDA-MB-468 cells to (*rac*/*meso*)-**4** (50 μM, 3-6 h) that did not result in immediate cellular rupture, TEM Z-Contrast sections (Figure 6B) reveal the generation of numerous low density vesicles (Figures 6B and S3-S6) within the cytoplasm characteristic of type III cell death – paraptosis, a primitive form of programmed cell death dependent upon protein transcription and translation, mediated by MAP kinase signaling[26].

Consistent with MAP kinase signal transduction, (*S,S*)-**4** (20 μM) strongly increased expression of total and phosphorylated EGFR (1 h – 24 h) in lysates of treated MDA-MB-468 cells (Figure 6C). After 12 h and 24 h exposure, powerfully up-regulated phosphorylated and total ERK 1 and 2 expression was also evident (Figures 6C and D). Screening lysates of MDA-MB-468 cells treated with (*S,S*)-**4** (20 μM) for 24 h against an array of key kinases corroborated strong up-regulation of ERKs 1 and 2 (Figure 6D). In HCT-116, AKT overexpression is observed in both cisplatin and titanocene **4** treated cells (24 h) which could be indicative of attempted survival in this cell line[27]. AKT signaling networks cascade to ERK1/2; indeed, in HCT 116 cells, following treatment with titanocene **4** only was up-regulation of both phosho ERK1/2 (at 3 h and 6 h) and total ERK 1/2 (6, 12 and 24 h) detected.

The ERK cascade represents a central signaling pathway regulating distinct and opposing cellular processes[28,29]. Herein, we propose that activation of receptor-mediated signal transduction leads directly to cell death through over production of the observed vacuoles and eventual membrane rupture. Such events are known to be triggered by selective activation of range of receptor-mediated pathways[26,30,31] in different cell types. MDA-MB-468 carcinoma cells, isolated from a patient with metastatic breast carcinoma represent a triple negative cell line expressing high levels of EGFR[32]. HCT 116 harbor mutant RAS rendering the MAP kinase cascade constitutively active[33].

Park *et al*. report vacuolization and dilated ER and mitochondria in MH-S murine alveolar macrophages by TiO_2 nanoparticles, and conclude that induced paraptosis and late onset apoptosis are the modes of action[34]. This may to be related to the cellular toxicity we observe, at 72 h exposure for samples rich in insoluble titanium compounds, but cannot account fully for the selective toxicity we see for the soluble intermediate ≤24 h.

Such behavior might be expected if hydrolysis of **4** is stepwise: chlorides initially (fast) and then, potentially, cyclopentadienyl units (slow) affording 'ligand-less' Ti-species whose subsequent uptake (endocytosis) is not enantiomer dependent. Endocytosis of TiO_2 20-30 nm nanospheres (after 24 h) in breast cancer SK-BR-3 cells is reported, resulting in average titanium concentrations of 28±5 picomols per cell as determined by ICP-MS, with some individual cells showing burdens >1000 picomol[35]. However, MDB-MB-468 breast cells treated with (*S,S*)-**4** (30 μM/3 h; the highest dose-time achievable without extensive lysis) revealed average titanium burdens per cell of only 3.3±0.3 femtomol (compared to 0.35

Published on 18 January 2016. Downloaded by University of Nottingham on 18/01/2016 16:44:32.

Metallomics Accepted Manuscript

View Article Online
DOI: 10.1039/C5MT00297D

femtomol for control, untreated cells). To specifically address the possibility that **4** is degraded to simple Ti^{4+} salts, its hydrolysis in dilute solution was studied and modeled by HPLC, MS and NMR techniques.

Published on 18 January 2016. Downloaded by University of Nottingham on 18/01/2016 16:44:32.

Metallomics Accepted Manuscript

View Article Online
DOI: 10.1039/C5MT00297D

Published on 18 January 2016. Downloaded by University of Nottingham on 18/01/2016 16:44:32.

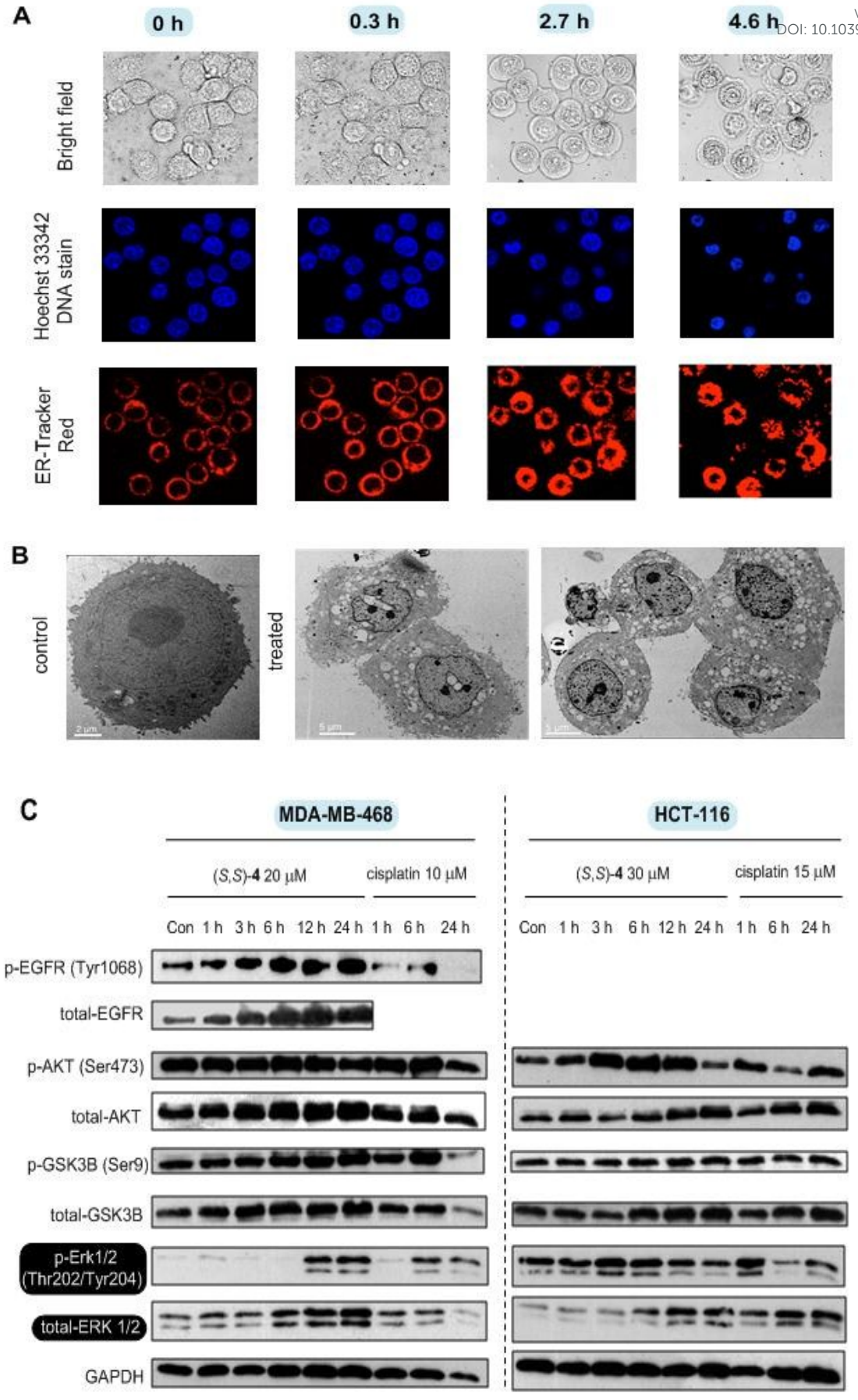

Metallomics Accepted Manuscript

View Article Online
DOI: 10.1039/C5MT00297D

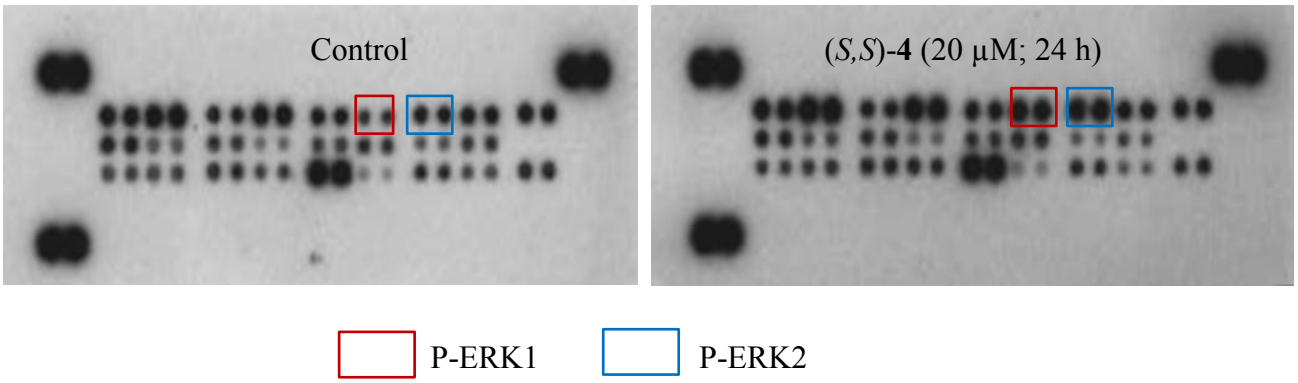

Figure 6. Paraptosis (type III cell death) induced by **4** in MDA-MB-468 and HCT 116 cells. A) Confocal microscopy MDA-MB-468 live cell imaging time-series studies after exposure to (*S*,*S*)-**4** (20 μM) revealed cytoplasmic vacuolization and ER swelling, followed by vacuole membrane rupture (osmotic lysis) and cell death. B) TEM imaging of MDA-MB-468 cells after exposure to (*rac*/*meso*)-**4** (50 μM; 3-6 h), revealed extensive vacuolization. C) Western blot assays of MDA-MB-468 and HCT-116 lysates following treatment of cells with (*S*,*S*)-**4** (20 or 30 μM; 1-24 h) or cisplatin (15 or 20 μM; 1, 6, 24 h). D) Lysates of MDA-MB-468 cells were subjected to the human phospho-MAPK array screen. Up-regulation of phosphorylated ERK1 and ERK2 was observed following treatment of cells with (*S*,*S*)-**4** (24 h; 20 μM).

Biophysics

The unsubstituted cyclopentadienyl complex Cp_2TiCl_2 (**1**) forms $[Cp_2Ti(OH)_n(OH_2)_m](Cl^-)_{2-n}$ mixtures (n = 1 - 2, n + m = 2) undergoing deprotonation / reprotonation events upon dissolution in aqueous media[36]. Hydrolytic Ti-Cp cleavage also occurs leading to poorly characterized, mixtures of Ti-complexes and free CpH. Correlation of biological effects to individual aquated titanium complexes is thus not practical for **1**. It is suggested that titanocenes containing monosubstituted cyclopentadienyls (specifically **3**; titanocene Y), are totally resistant to Ti-C_5H_4R hydrolysis[37] potentially simplifying the number of aqueous Ti-species present. However, to the best of our knowledge, no definitive data have been published to support such assertions. Thus, we studied the aqueous dissolution behavior of **4** under conditions close to the biological and imaging studies above (0-72 h and μM aqueous concentrations) by HPLC, MS and NMR techniques.

Initial biological screening stock solutions (20 mM) of **4** were attained by dissolution in DMSO at room temperature. The 800 MHz ^{1}H NMR spectra of both *rac* and *meso*-**4** (200 μM) in d_6-DMSO is very similar to that in anhydrous non-coordinating $CDCl_3$ (average signal shift +0.1 ppm; deviation range on individual signals: +0.0 to +0.5 ppm) and invariant over 48 h. Chiral HPLC analyses of such solutions provide only elution of (*R*,*R*)-, (*S*,*S*)- or *meso*-**4** bands (correlating with the sample used and identical with authentic samples). These observations strongly suggest no ionization of chloride or Cp^R groups takes place in DMSO prior to dilution with RPMI medium to give 200 μM samples of **4** containing 1% v/v aqueous d_6-DMSO. The latter nominal 200 μM aqueous samples, while appearing clear to the naked eye, contain colloidal suspensions of **4** on the basis that: (i) unfiltered samples give a +ESI MS signal at *m/z* 509 with a $^{35/37}$Cl isotope pattern for $[(Cp^R)_2TiCl]^+$ (for **4** - Cl), which is absent in equivalent filtered or HPLC eluted samples. (ii) Model dilution of 20 mM (*S*,*S*)-**4** in

Published on 18 January 2016. Downloaded by University of Nottingham on 18/01/2016 16:44:32.

Metallomics Accepted Manuscript

View Article Online
DOI: 10.1039/C5MT00297D

d_6-DMSO to 200 μM in D_2O provides ^{1}H 800 MHz initial NMR spectra that are broad and characteristic of undissolved material (Supplementary Information). On standing, 200 μM colloidal suspensions of (*S,S*)-**4** in RPMI lead to formation of a new homogeneous intermediate **I** as evidenced by its elution in LCMS (t_r 3.0 min). The intermediate **I** ionizes as *m/z* 491 which was assigned to $[Cp^R_2Ti(OH)]^+$. Treatment of solutions containing the intermediate **I** with methanol led to immediate qualitative formation of a signal at *m/z* 505 in +ESI MS. Such behavior is consistent with $[Cp^R_2Ti(OMe)]^+$ formation through solvent exchange. Over time the concentration of the $[Cp^R_2Ti(OH)]^+$ **I** intermediate in 1% v/v DMSO/RPMI first maximizes (t_{max} = 1.2 h) and then decays, over 24 h, with re-formation of an insoluble colloid based on reduction of signal intensity in the LCMS analysis. Analysis of the unfiltered residue reveals a +ESI MS signal at *m/z* 981 assigned as $[2 \times Cp^R_2Ti(O)+H^+]$.

The formation of intermediate **I** could be modeled by dissolution of (*R,R*)-**4** to nominal 200 μM in 1% v/v d_6-DMSO/D_2O at room temperature. The initial insolubility of (*S,S*)-**4** was confirmed, as was the generation (and subsequent decay, $t_{½}$ ~ 1.7 h) of the same soluble intermediate **I** (also ionizing as *m/z* 491/492). When the concentration of intermediate **I** is maximized (*ca.* 80 μM) the 800 MHz ^{1}H NMR spectrum is fully in accord with the presence of a 'Cp^R_2Ti' core with no cyclopentadienyl cleavage (Figure 7A). The soluble intermediate's kinetic behavior could also be modelled by consecutive equilibrating first order reactions simulating both the growth of **I** and its subsequent decay well (Figure 7B, quality of fit R^2 0.98, see Supplementary Information). The hypothesis that **I** is Lewis acidic $[Cp^R_2Ti(OH)]^+$ and that it can bind external ligands (H_2O and other donor ligands) was tested by additional runs in 20% v/v d_6-DMSO:D_2O. The lifetime of the intermediate increased 5-fold ($t_{½}$ ~9.5 h, with increased maximum intermediate concentration of 200 μM). This supports Lewis base exchange forming $[Cp^R_2Ti(OH)(DMSO)]^+$ at increased DMSO concentration. However in 1% v/v DMSO/aqueous conditions all evidence (HPLC, MS, NMR) supports $[Cp^R_2Ti(OH)(H_2O)]Cl$ as the identity of the major aqueous species **I** (>90%) present during the observation of enantiomer differentiated paraptosis. The decay of **I** is apparently due to deprotonation leading to neutral product $(Cp^R)_2Ti{=}O$ which is not soluble in water – rather than hydrolysis to non Cp^R containing species. Both **I**'s kinetic behavior (apparent equilibrium with an insoluble product) and observation of traces of its dimerization product $[\{(Cp^R)_2Ti{=}O\}_2+H]^+$ *m/z* 981 in the +ESI MS are in accord with this hypothesis. Importantly, within the time periods employed in our experiments (0-60 h) we could detect *no* free Cp^RH hydrolysis products (down to 1-2 μM) in NMR experiments – indicating that the situation for **4** is very different to that of the parent **1**. The overall behavior of **4** upon aqueous dilution and ions detected by MS and LCMS during the starting material (colloidal), intermediate (truly homogeneous) and product (colloidal) phases of the hydrolyses of (*S,S*)-**4** are summarized in Figure 8.

Published on 18 January 2016. Downloaded by University of Nottingham on 18/01/2016 16:44:32.

Metallomics Accepted Manuscript

View Article Online
DOI: 10.1039/C5MT00297D

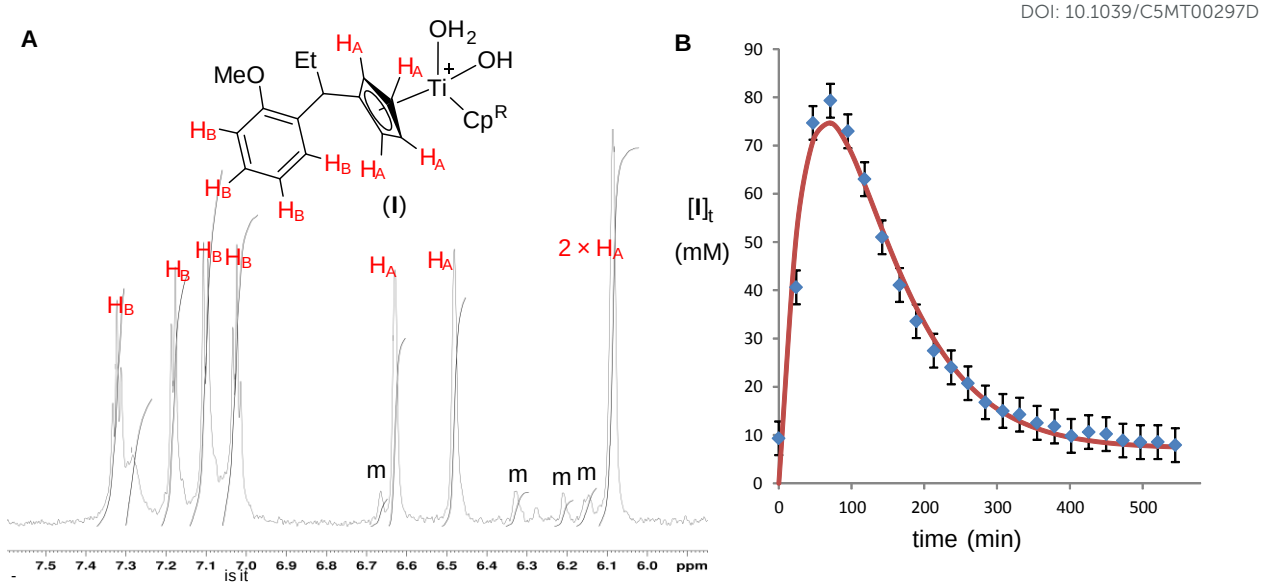

Figure 7. A) Partial ^{1}H NMR spectrum (6-7.5 ppm) of the truly homogeneous intermediate **I** (ca. 80 mM) resulting from dissolution of **4** in 1:99 d_6-DMSO/D_2O. Signals attributable other functional groups within **I** could also be detected: **I**δ_H 7.33, 7.18, 7.10, 7.03 (H_b) 6.63, 6.48, 6.08 (2H) (*CH*C_5H_4), 3.84 (OMe), 1.90, 1.80 and 0.71 (3H) (Et) (see SI). Traces of *meso*-diasteriomer (m) can also be seen in the spectrum as the *rac*/*meso* ratio of the (*R*,*R*)-**4** (>99:1 e.r.) used was 85:15. The broad signal at δ_H 7.28 grows in with formation of **I** and may indicate aggregation before precipitation of insoluble product (**P**). **B**) Fit of the concentration of **I** vs. time after first dissolution of colloidal (*R*,*R*)-**4** nominally 200 mM in 1:99 d_6-DMSO/D_2O to equilibrating first order reactions using the equations of Moore and Pearson.

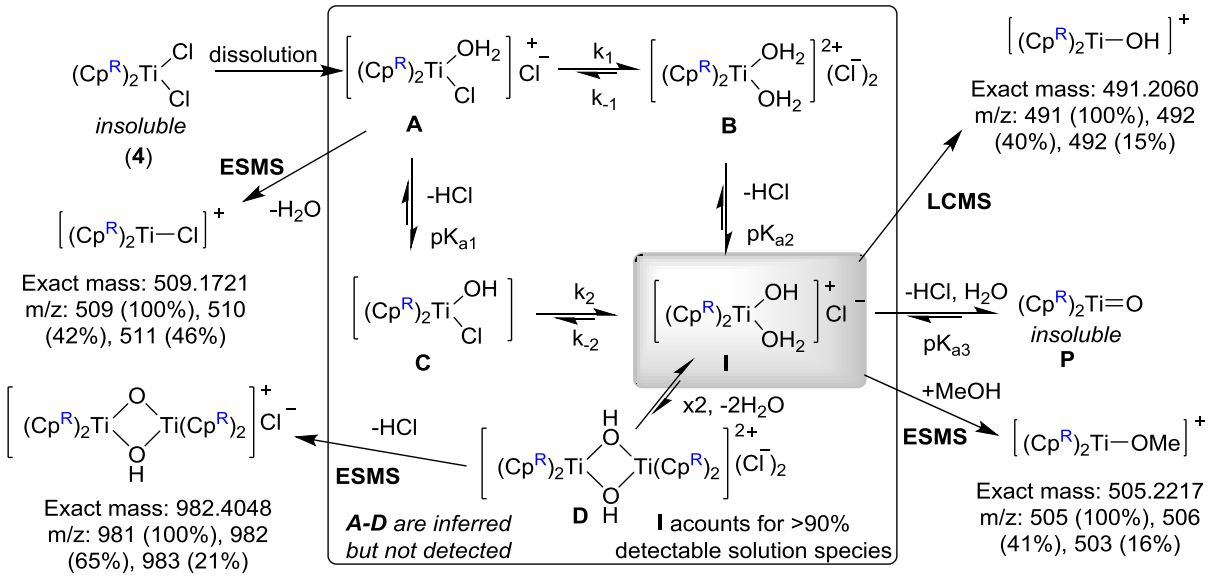

Figure 8. Observed and inferred processes on dissolution of **4** in aqueous media.

Published on 18 January 2016. Downloaded by University of Nottingham on 18/01/2016 16:44:32.

Metallomics Accepted Manuscript

View Article Online
DOI: 10.1039/C5MT00297D

Published on 18 January 2016. Downloaded by University of Nottingham on 18/01/2016 16:44:32.

The lack of free Cp^R in cultures containing **4**, very low Ti intracellular concentrations and enantiomer dependent biology are not in accord with significant accretion of cyclopentadienyl free Ti^{4+} within our cell lines. Such suggestions originally arose from exposure of dead tissue samples to massive excesses of **1** and in apparent low level EELS Ti signals detected in biopsy samples[38,39]. In reproducing the latter we find the titanium EELS signal is reproducibly coincident with a background artefact, and at best, low Ti concentrations are present with no aggregation of TiO_2-like species above 1 nm diameter within MDA-MB-468 cells detectable (3-6 h) (Supplementary Information). Transferrin has been suggested as mechanism for Ti^{4+} transport into cells[40,25], but recent studies[41] show it had no significant positive effect on the anti-cancer activity of **1** and other Ti-based agents. If titanium transport into MDA-MB-468 does operate in our system the resultant aggregates would have to be both very small (<1 nm) and numerous (>10^{10}) per cell to avoid our detection limits. In known paraptotic TiO_2-triggered systems the Ti-particles are typically 5-500 nm in size[34,42] and these would have been detected by our equipment. Based on the low levels of titanium per cell, the alternative possibility of titanium-based paraptotic signal transduction makes perfect sense. Indeed, evidence of signal transduction pathways activated to produce cytoplasmic induced paraptosis by (*S,S*)-**4** is presented herein. Conversely, slow endocytosis of colloidal $Cp^R{}_2Ti(O)$, precipitated from soluble **I** over time, would also be fully concordant with the lack of enantiomer recognition we see at 72 h when screening **4** in MTT assays. Finally, exchange of $[Cp^R{}_2(OH)(H_2O)]^+$ **I** to longer lived $[Cp^R{}_2Ti(OMe)(MeOH)]^+$ also provides a rational for the, otherwise poorly explained, increased toxicity of **1** when it is pre-treated with methanol[43].

In summation, in the period during which paraptosis was observed, soluble *m/z* 491 $[Cp^R{}_2Ti(OH)]^+$ was the only cyclopentadienyl intermediate observed (>90% of total signal). No free ligand *m/z* 214 was detected in LCMS studies ≤24 h. Addition of MeOH to solutions containing m/z 491 $[Cp^R{}_2Ti(OH)]^+$ led to its rapid complete conversion to *m/z* 505 $[Cp^R{}_2Ti(OMe)]^+$. All of these observations are in accord with $[Cp^R{}_2(OH)(H_2O)]^+$ **I** being the major solution species present under conditions leading to biological activity.

Conclusions

(*S,S*)-**4**, (*R,R*)-**4** and (*rac,meso*)-**4** revealed growth inhibitory activity with equivalent potency to cisplatin in mammary, colorectal and pancreatic carcinoma cell lines. Unlike cisplatin, selectivity (2-5-fold) for cancer cell lines over MRC5 fibroblasts was detected. Low tissue (and myesosuppressive) toxicity (compared with Pt-based drugs) would render titanocene anticancer agents candidates for combination therapy.

In clonogenic assays, survival and colony formation after 24 h exposure demonstrated enantiomer selectivity: (*S,S*)-**4** ~2-fold greater potency, corroborating previous MTT assays performed following 24 h exposure of cancer cell lines to titanocene **4** enantiomers[16].

In stark contrast to cisplatin, titanocene **4** negligibly perturbed MDA-MB-468 and HCT 116 cell cycle, did not cause DNA double strand breaks and failed to trigger significant apoptosis. Evidence strongly advocates cell death by paraptosis following treatment of cancer cells to titanocene **4**: extensive cytoplasmic vacuolization accompanied by up-regulated expression of proteins integral to EGFR, MAP kinase and AKT signal transduction preceded membrane rupture and cell death. Appearance of these dramatic cellular morphological modifications is concurrent with maximized concentrations of a soluble intermediate **I** whose NMR, MS and kinetic behavior is concordant with $[Cp^R{}_2Ti(OH)\ )(H_2O)]^+$.

Metallomics Accepted Manuscript

View Article Online
DOI: 10.1039/C5MT00297D

The history of titanocene dichloride thereaputic agents is populated with conflicting suggestions for biological pathways that have subsequently proved tangential to modes of action in particular cell lines. Unpicking the specific biological chaperone(s) that bind(s) the key hydroxyl active intermediate triggering paraptosis will require extensive systematic correlation of target binding to cancer cell growth inhibition across a wide family of *enantiomeric* substituted titanocenes to ensure complete veracity of the biological target(s) involved. This is the next goal of our research. However, we can conclude that the single enantiomeric titanocenes are highly appropriate and powerful tools for such approaches, and may herald the possibility of titanocene-based therapy through paraptosis.

Methods.

Test agents

Titanocene enantiomers **4** were synthesized according to a recently published method[16]. Cisplatin was purchased from Sigma-Aldrich.

Cell culture

Cells were passaged twice weekly upon reaching 70-80% confluency. Cells were sub-cultured in RPMI 1640 medium containing sodium bicarbonate supplemented (2 g/L), L-glutamine (0.3 g/L) and 10% heat-inactivated foetal bovine serum (FBS).

MTT assay

The 3-[4,5-dimethylthiazol-2-yl]-2,5-diphenyl tetrazolium bromide (MTT) assay was used as described[44] to assess the ability of test agents to inhibit cell growth and/or evoke cytotoxicity. MTT assays were performed at the time of agent addition (T zero) and following 72h exposure of cells to test agents.

Clonogenic assay

The clonogenic cell survival test was adopted to measure the ability of a single cell to survive brief exposure to test agent and maintain proliferative potential to form progeny colonies. The assay was performed as previously described[44].

Cell cycle analysis

Cell cycle analyses were performed according to Nicoletti et al[45]. Cells were seeded in cell culture dishes at densities of $3\text{-}5\times10^5$ cells/dish in 10 mL medium. Following treatment, cells were harvested and pelleted by centrifugation then re-suspended in 0.5-1 mL fluorochrome solution (50 µg/mL propidium iodide (PI), 0.1 mg/mL ribonuclease A, 0.1% v/v Triton X-100, and 0.1% w/v sodium citrate in dH_2O). Cells were stored overnight in the dark at 4 ^oC. Cell cycle analyses were performed on a Beckman Coulter FC500 flow cytometer. EX- PO32 software was used to analyze data.

Dual determination of γH2AX foci and cell cycle perturbation

For dual γH2AX detection of DNA double strand breaks and cell cycle analysis cells were

Published on 18 January 2016. Downloaded by University of Nottingham on 18/01/2016 16:44:32.

Metallomics Accepted Manuscript

View Article Online
DOI: 10.1039/C5MT00297D

seeded in cell culture dishes at densities of 3-5×10^5 cells/dish in 10 mL medium. Following 72 h treatment, cells were harvested and pelleted by centrifugation, re-suspended and washed (2x) in PBS, pelleted by centrifugation and fixed in 500 µL 1% methanol-free formaldehyde in PBS (5 min; room temperature). Cells were permeabilized by adding 500 µL 0.4% Triton-X-100in PBS. FBS (1% in PBS; 1 mL) was added to cells with gentle mixing before incubation at room temperature for 30 min. Cell suspensions were centrifuged and supernatants aspirated. 1^o Ab solution (200 µL) was added to each tube and samples were incubated for 1.5 h. PBS (1 mL) was added and samples were centrifuged and supernatants discarded. 2^o Ab was introduced (200 µL) and samples incubated for 1 h at room temperature before addition of 1 mL PBS. Samples were centrifuged and supernatant again discarded. Cells were resuspended in PBS containing 300 µL 50 µg/mL PI and 0.1 mg/mL RNaseA. Analyses of cells by flow cytometry followed >10 min incubation.

Annexin V apoptosis assay

Reagents used were Annexin V-FITC Ab, 1× annexin binding buffer (1:10 dilution 10× annexin binding buffer in dH_2O), and PI solution (50 µg/mL in PBS). Cells (1×10^5 cells/well) were seeded in 6 well plates are incubated overnight before treatment with test agent (24 and 72 h). Cells were trypsinised and collected in FACS tubes then kept on ice for 10 min. Annexin-V-FITC (5µL) plus 100 µL 1× annexin-V buffer were added to cells after centrifugation. After 15 min incubation in the dark at room temperature, PI (10 µL; 50 µg/mL in PBS) plus 400 µL annexin-V buffer were added. Samples were protected from light and kept on ice for 10 min before analysis on a Beckman Coulter FC500 flow cytometer. EX-PO32 software was used to analyze data.

Confocal microscopy

MDA-MB-468 cells (3×10^5) were seeded over coverslips in glass petri dishes in 2 mL RPMI supplemented with 10% FBS. Cells were incubated at 37 ^{o}C for 24 h, to allow attachment, prior to titanocene **4** exposure (3-6 h). Medium was aspirated, cells washed (2×; HBSS) and DNA stained (4 µM Hoeschst; 37 ^{o}C; 30 min). Solution was aspirated, cells washed and re-stained with 1 µM ER-Tracker red for 20 min. Staining solution was aspirated, cells washed and bathed in medium before viewing by fluorescence confocal microscopy (Zeiss LSM710 confocal instrument; Zeiss observer with PlanApo 40x/1.30 oil objective. Images were captured running Zen software.

Transition electron microscopy

A JEOL 2100F TEM instrument equipped with Gatan Orius high sensitivity cameras was used. Atomic contrast HAADF imaging was performed using the JEOL Digital STEM system and Electron Energy Loss Spectroscopy (EELS) was *via* a Gatan Tridiem Filter. The TEM was also equipped with a state-of-the-art windowless X-MaxN 100TLE EDX detector. The system was equipped with a Gatan 914 liquid nitrogen cooled holder, for stabilizing heat-sensitive samples.

This configuration allowed analysis on the nm scale at concentrations ≥0.01% for the typical sample thickness and acquisition time used in this study. Concentrations of Ti 1 part in 10,000 C, or Ti content aggregates > 1nm would be detected if present within the cell.
MDA-MB-468 cells were cultured in thermanox coverslips in 6 well plates. Cells were allowed to attach for 24 h before exposure to 50 µM **4** ≤6 h. In order to achieve maximum

Published on 18 January 2016. Downloaded by University of Nottingham on 18/01/2016 16:44:32.

Metallomics Accepted Manuscript

View Article Online
DOI: 10.1039/C5MT00297D

dose-time exposure and to maximize the opportunity for uptake and detection of titanium, *meso/rac*-**4** was used. Untreated control cells and titanocene treated cells were fixed with 3% EM Glutaraldehyde in 0.1 M cacodylate buffer for 1 h at 4 ^{o}C. Fixed cells were then washed with 0.1 M cacodylate buffer followed by post-fixation with 1% aqueous osmium tetroxide for 30 min. Samples were washed with dH_2O for 5 min followed by serial dehydration in ethanol (50%; 70%; 90%; 100%). The coverslips were then transferred to a clean porcelain dish and washed (2 x 5 min) with 100% propylene oxide. Resin (25 mL araldite CY212 resin, 15 mL agar 100 resin, 55 mL DDSA, 2 mL dibutyl phthalate and 1.5 mL DMP 30) was prepared and samples were infiltrated with this resin mixture. Samples were then embedded by inverting the coverslip on a ballistic electron emission microscopy (BEEM) capsule filled with the resin so that only the cell layer was embedded in the resin. The sample was then left in an embedding oven for 48 h at 60 ^{o}C. The resin sample was then sectioned using an ultramicrotome (200 nM thickness) and embedded in a copper mesh grid and stained with uranyl acetate/lead citrate.
Imaging and elemental analysis in the TEM was performed on microtomed sections, both on sections supported on copper mesh grid only – i.e. sample against vacuum – or on sections additionally supported on newly commercially available graphene oxide support grids (Agar Scientific). The graphene oxide films provide a charge and heat conductive support that stabilizes the sample under the electron beam, allowing longer acquisition times[46].

Inductively coupled plasma mass spectrometry (ICP-MS)

Cells were grown as described in 5 mL RPMI-1640 medium supplemented with 10% FBS. No titanium above background levels (0.3 ppb) could be detected in either component. Typically, ~5 × 10^5 MDA-MB-468 cells were grown in the presence of (*S,S*)-**4** (30 μM), or vehicle control. Higher concertation-time loadings of (*S,S*)-**4** could not be used without engendering degradative lysis. Following 4 h exposure, growth media were removed to separate vials and cells were washed with 2 × 2 mL PBS, and the wash buffer was added to the appropriate vials containing the separated supernatant medium. The remaining cells were then trypsinized (1mL) and pelleted by centrifugation; the supernatant trypsin solution was added to the appropriate wash vial. The cell pellet was once more washed (PBS; 1 mL). Pelleted cells were digested (16% w/w HNO_3, 3 mL, 95 ^{o}C, 2 h) and diluted with MilliQ water to a final volume of 15 mL. The combined wash solutions were similarly digested. Analyses were conducted on a Thermo Scientific iCAP QC.

Western blot

MDA-MB-468 and HCT 116 cells were seeded in dishes (100×20 mm) at a density of 1-2 x 10^6 per dish, allowed 24 h to attach, and exposed to test agent (1 – 24 h). Following required exposure, cells were lysed in NP-40 lysis buffer supplemented with PhosSTOP Phosphatase Inhibitor Cocktail (Roche Applied Science) and COMPLETE-mini Protease Inhibitor Cocktail (Roche Applied Science). Cell debris was removed by centrifugation at 14,000 x g for 5 min. Protein concentrations were determined using QuickStart Bradford Assay (Bio-Rad, Hemel Hempstead, UK). Cell lysate proteins (50 μg) were separated by SDS-polyacrylamide gel electrophoresis and then transferred to a nitrocellulose membrane. Membranes were probed with the following antibodies, all purchased from Cell Signaling Technologies: p-EGFR (Tyr1068), total-EGFR, p-AKT (Ser473), total-AKT, p-GSK3β (Ser9), total-GSK3β, p-ERK1/2(Thr202/Tyr204), total-ERK1/2 and GAPDH.

Published on 13 January 2016. Downloaded by University of Nottingham on 18/01/2016 16:44:32.

Metallomics Accepted Manuscript

View Article Online
DOI: 10.1039/C5MT00297D

Published on 18 January 2016. Downloaded by University of Nottingham on 18/01/2016 16:44:32.

Relative protein phosphorylation

Relative protein phosphorylation levels of 24 kinases were detected simultaneously using the Human Phospho-Mitogen-activated Protein Kinase (MAPK) Antibody Array (Catalog # ARY002B) from R&D systems according to the manufacturer's instructions. Briefly, MDA-MB-468 cells were seeded in Corning® tissue-culture treated culture dishes (100 mm x 20 mm; 1 x 10^6 per culture dish). Cells were allowed to attach overnight and left untreated or treated with (*S,S*)-**4**, 20 μM, for 24 h. Cells were rinsed with PBS followed by solubilization in lysis buffer by gently rocking at 4°C for 30 min. Cell lysates were then microcentrifuged at 14,000 x g for 5 min and then the supernatant was transferred into a clean eppendorf tube. Quantitation of sample protein concentration was carried out using QuickStart Bradford Assay (Bio-Rad, Hemel Hempstead). Aliquots of the lysates were then stored frozen at −80 °C. Membranes were blocked with the kit's blocking buffer at room temperature for 1 h on a rocking platform shaker. Whilst membrane blocking, the 2 cell lysate samples (MDA-MB-468 – 24 h control and 24 h (*S,S*)-**4** 20 μM) were diluted with array buffer followed by a cocktail of biotinylated detection Abs. The sample was mixed and incubated at room temperature for 1 h. The sample/antibody mixture was placed on the membrane and the dish containing the membrane was incubated overnight at 4°C on a rocking platform shaker. Thereafter, cocktails of biotinylated detection antibodies were added at room temperature for 1 h. Phosphorylated proteins were revealed using streptavidin-HRP/Chemi Reagent Mix and autoradiography films (Amersham Hyperfilm ECL, GE Healthcare Life Sciences, Buckinghamshire, UK).

NMR spectroscopy

Samples of (*S,S*)- or (*R,R*)-**4** (200 μM in D_2O/d_6-DMSO, 99:1) for combined 800 MHz NMR were prepared as described for preparation of stock solutions of **4** used in biological and MS studies, except that D_2O, not RPMI-1640, was used. Attempts to directly study samples in RPMI-1640 led to the observation of very broad signals. For NMR studies (*R,R*)-**4** (0.6 mg, 1.1 μmol) was dissolved in spectroscopic grade d_6-DMSO (55 μL) to afford a nominal 20 mM top stock solution. An aliquot of this (15 μL, 0.3 μmol) was added to 1485 μL standard solution (67 μM) of Na-TMSP-d_4 [3-(trimethylsilyl)-2,2',3,3'-tetradeuteropropionic acid, sodium salt] in D_2O and the time noted. A sample of this nominal 200 μM solution of (*R,R*)-**4** containing Na-TMSP-d_4 internal standard (67 μM) was immediately transferred to the 800 MHz spectrometer and the latter set to attain ^{1}H NMR spectra every 25 min (probe temperature 25±0.2 ^{o}C). The limit of detection of soluble species was ~1 μM. Controlled spiking experiments with Cp^RH confirmed identification of free ligand at 1 μM, but none was detected in the period of observation (0-60 h).

Mass Spectrometry

In a manner identical to preparation of sample dilutions for biological studies, 200 μM (*S,S*)-**4** was prepared in RPMI-1640 (pH 6.9 to 7.2) using freshly prepared 20 mM DMSO top stock. Mass spectrometry provided insight into species derived from (*S,S*)-**4**. Liquid Chromatography Mass Spectrometry (LCMS) assayed only truly homogeneous species (fine colloidal suspensions, even those apparently clear to the naked eye, are not eluted making this a powerful way to separate genuine solution Cp^RTi species from degradation events). Direct injection of sample for Electrospray Mass Spectrometry (ESMS) allowed detection of both homogeneous and colloidal species. Ions from the latter could be identified by the presence of extra signals in the paired mass spectra.

Metallomics Accepted Manuscript

View Article Online
DOI: 10.1039/C5MT00297D

LCMS was carried out using an Agilent 1260 Infinity HPLC with a 6120 Quadrupole mass spectrometer. A Waters Sunfire C18 3.5µm 2.1 x 30 mm column was used; mobile phase 1 comprised 0.1% formic acid in water; mobile phase 2 comprised 0.1% formic acid in acetonitrile. Experiments were performed at 40 ^{o}C with a flow rate of 0.8 mL min^{-1}, gradient 5-95 % mobile phase 2 over 3.5 minutes with UV detection at 210-400 nm reported at 254 nm. MS ionisation by ESI operated in positive ion mode. Samples were collected every 10 min ≤ 6 h depending on the rate of change in the speciation. Direct ESMS was conducted on a Bruker microTOF instrument in 1% DMSO in D_2O.

Published on 18 January 2016. Downloaded by University of Nottingham on 18/01/2016 16:44:32.

Metallomics Accepted Manuscript

View Article Online
DOI: 10.1039/C5MT00297D

References

1. P. Kopfmaier and H. Kopf, *Anticancer Res*, 1986, **6**, 227-233.
2. A. Korfel, M. E. Scheulen, H. J. Schmoll, O. Grundel, A. Harstrick, M. Knoche, L. M. Fels, M. Skorzec, F. Bach, J. Baumgart, G. Sass, S. Seeber, E. Thiel and W. E. Berdel, *Clin Cancer Res*, 1998, **4**, 2701-2708.
3. C. V. Christodoulou, D. R. Ferry, D. W. Fyfe, A. Young, J. Doran, T. M. T. Sheehan, A. Eliopoulos, K. Hale, J. Baumgart, G. Sass and D. J. Kerr, *J Clin Oncol*, 1998, **16**, 2761-2769.
4. K. Mross, P. Robben-Bathe, L. Edler, J. Baumgart, W. E. Berdel, H. Fiebig and C. Unger, *Onkologie*, 2000, **23**, 576-579.
5. N. Kroger, U. R. Kleeberg, K. Mross, L. Edler, G. Sass, D. K. Hossfeld and P. I. I. S. G. A. M. Onc, *Onkologie*, 2000, **23**, 60-62.
6. G. Lummen, H. Sperling, H. Luboldt, T. Otto and H. Rubben, *Cancer Chemoth Pharm*, 1998, **42**, 415-417.
7. I. Fichtner, C. Pampillon, N. J. Sweeney, K. Strohfeldt and M. Tacke, *Anti-Cancer Drug*, 2006, **17**, 333-336.
8. J. B. Waern, C. T. Dillon and M. M. Harding, *J Med Chem*, 2005, **48**, 2093-2099.
9. J. B. Waern, H. H. Harris, B. Lai, Z. H. Cai, M. M. Harding and C. T. Dillon, *J Biol Inorg Chem*, 2005, **10**, 443-452.
10. M. L. Guo and P. J. Sadler, *J Chem Soc Dalton*, 2000, 7-9.
11. M. L. Guo, H. Z. Sun, H. J. McArdle, L. Gambling and P. J. Sadler, *Biochemistry-Us*, 2000, **39**, 10023-10033.
12. C. V. Christodoulou, A. G. Eliopoulos, L. S. Young, L. Hodgkins, D. R. Ferry and D. J. Kerr, *Brit J Cancer*, 1998, **77**, 2088-2097.
13. A. D. Tinoco, E. V. Eames and A. M. Valentine, *J Am Chem Soc*, 2008, **130**, 2262-2270.
14. M. Pavlaki, K. Debeli, I. E. Triantaphyllidou, N. Klouras, E. Giannopoulou and A. J. Aletras, *J Biol Inorg Chem*, 2009, **14**, 947-957.
15. J. Fernandez-Gallardo, B. T. Elie, F. J. Sulzmaier, M. Sanau, J. W. Ramos and M. Contel, *Organometallics*, 2014, **33**, 6669-6681.
16. M. B. Cini, T. D.; Woodward, S.; Lewis, W., *Angewandte Chemie International Edition*, 2015.
17. A. D. Tinoco, H. R. Thomas, C. D. Incarvito, A. Saghatelian and A. M. Valentine, *P Natl Acad Sci USA*, 2012, **109**, 5016-5021.
18. N. Poklar, D. S. Pilch, S. J. Lippard, E. A. Redding, S. U. Dunham and K. J. Breslauer, *P Natl Acad Sci USA*, 1996, **93**, 7606-7611.
19. G. N. Rudd, J. A. Hartley and R. L. Souhami, *Cancer Chemoth Pharm*, 1995, **35**, 323-326.
20. Fritsche, *Oncogene*, 1993, **8**, 2605-2605.
21. S. Cuffe, C. M. Dowling, J. Claffey, C. Pampillon, M. Hogan, J. M. Fitzpatrick, M. P. Carty, M. Tacke and R. W. G. Watson, *Prostate*, 2011, **71**, 111-124.
22. K. O'Connor, C. Gill, M. Tacke, F. J. K. Rebmann, K. Strohfeldt, N. Sweeney, J. M. Fitzpatrick and R. W. G. Watson, *Apoptosis*, 2006, **11**, 1205-1214.
23. L. J. Kuo and L. X. Yang, *In Vivo*, 2008, **22**, 305-309.
24. J. H. Bannon, I. Fichtner, A. O'Neill, C. Pampillon, N. J. Sweeney, K. Strohfeldt, R. W. Watson, M. Tacke and M. M. Mc Gee, *Brit J Cancer*, 2007, **97**, 1234-1241.
25. U. Olszewski and G. Hamilton, *Anti-Cancer Agent Me*, 2010, **10**, 302-311.
26. S. Sperandio, K. Poksay, I. de Belle, M. J. Lafuente, B. Liu, J. Nasir and D. E. Bredesen, *Cell Death Differ*, 2004, **11**, 1066-1075.
27. J. Zhang, L. L. Zhang, L. Shen, X. M. Xu and H. G. Yu, *Oncol Lett*, 2013, **5**, 756-760.
28. Z. Yao and R. Seger, *Biofactors*, 2009, **35**, 407-416.
29. Y. D. Shaul and R. Seger, *Bba-Mol Cell Res*, 2007, **1773**, 1213-1226.
30. J. Fombonne, L. Padron, A. Enjalbert, S. Krantic and A. Torriglia, *Apoptosis*, 2006, **11**, 367-375.

Published on 18 January 2016. Downloaded by University of Nottingham on 18/01/2016 16:44:32.

Metallomics Accepted Manuscript

View Article Online
DOI: 10.1039/C5MT00297D

31. Y. Wang, X. T. Li, L. Wang, P. G. Ding, Y. M. Zhang, W. L. Han and D. L. Ma, *J Cell Sci*, 2004, **117**, 1525-1532.
32. R. Cailleau, M. Olive and Q. V. J. Cruciger, *In Vitro Cell Dev B*, 1978, **14**, 911-915.
33. P. C. Schroy, S. Brownshimer, K. Kim, K. A. Johnson, M. J. Murnane, S. Yang, M. J. Obrien, W. P. Carney and H. Z. Kupchik, *Cancer*, 1995, **76**, 201-209.
34. E. J. Park, S. Y. Lee, G. H. Lee, D. W. Kim, Y. Kim, M. H. Cho and J. H. Kim, *Toxicol Lett*, 2014, **230**, 69-79.
35. J. T. Rashkow, S. C. Patel, R. Tappero and B. Sitharaman, *J R Soc Interface*, 2014, **11**.
36. J. H. Toney and T. J. Marks, *J Am Chem Soc*, 1985, **107**, 947-953.
37. J. Schur, C. M. Manna, A. Deally, R. W. Koster, M. Tacke, E. Y. Tshuva and I. Ott, *Chem Commun*, 2013, **49**, 4785-4787.
38. P. Kopfmaier and D. Krahl, *Naturwissenschaften*, 1981, **68**, 273-274.
39. P. Kopfmaier and D. Krahl, *Chem-Biol Interact*, 1983, **44**, 317-328.
40. K. M. Buettner and A. M. Valentine, *Chem Rev*, 2012, **112**, 1863-1881.
41. T. Suzuka, M. Ogasawara and T. Hayashi, *J Org Chem*, 2002, **67**, 3355-3359.
42. K. T. Thurn, H. Arora, T. Paunesku, A. G. Wu, E. M. B. Brown, C. Doty, J. Kremer and G. Woloschak, *Nanomed-Nanotechnol*, 2011, **7**, 123-130.
43. M. Ravera, C. Cassino, E. Monti, M. Gariboldi and D. Osella, *J Inorg Biochem*, 2005, **99**, 2264-2269.
44. V. J. Raja, K. H. Lim, C. O. Leong, T. S. Kam and T. D. Bradshaw, *Invest New Drug*, 2014, **32**, 838-850.
45. I. Nicoletti, G. Migliorati, M. C. Pagliacci, F. Grignani and C. Riccardi, *J Immunol Methods*, 1991, **139**, 271-279.
46. R. S. Pantelic, J. C. Meyer, U. Kaiser and H. Stahlberg, *Solid State Commun*, 2012, **152**, 1375-1382.

Published on 18 January 2016. Downloaded by University of Nottingham on 18/01/2016 16:44:32.

Metallomics Accepted Manuscript

View Article Online
DOI: 10.1039/C5MT00297D

Acknowledgments. We thank the University of Nottingham for a studentship and the support of the Edith Johnson Bequest (M. Cini). NMR Facilities were funded by the University of Nottingham under the CIF (Capital Investment Framework) initiative. We thank A. Kuruppu, D. McLean and S.Young for their assistance with Western blots, TEM sectioning and ICP-MS respectively.

Author contributions: M.C., T.D.B. and S.W. conducted all synthetic and biological research; M.C., H.W., M.W.F., T.D.B., and S.W. analyzed data; T.D.B., M.C. and S.W. wrote the manuscript.

Published on 18 January 2016. Downloaded by University of Nottingham on 18/01/2016 16:44:32.

Metallomics Accepted Manuscript